

# RECENT RESULTS FROM THE ELECTRON BEAM PROFILE MONITOR AT THE SWISS LIGHT SOURCE

Å. Andersson, A. Lüdeke, M. Rohrer, V. Schlott, A. Streun, PSI, Villigen, Switzerland  
Oleg Chubar, SOLEIL, Gif-sur-Yvette, France

## Abstract

Two different methods of beam profile measurements using a) visible-to-UV range synchrotron radiation and b) X-ray synchrotron radiation have been realized in a single diagnostics beam line at the Swiss Light Source (SLS). In the visible-to-UV case the vertically polarized synchrotron radiation renders an image heavily influenced by inherent emission and diffraction effects of synchrotron radiation. This nevertheless turns out to be an advantageous influence when determining rms beam profiles below 10  $\mu\text{m}$ . However, high-precision wave-optics based calculations of the synchrotron light characteristics need to be performed (SRW-code) to ensure correct interpretation of the measured profiles. The visible-to-UV branch has a few built-in features allowing numerous cross-checks of the SRW-model. Surprisingly, wave-optics based calculations are also applicable, and required, for the X-ray pinhole camera setup. We briefly discuss the advantage of applying two different measuring techniques at the same source point. In total, for standard user operation at the SLS, the beam line has helped to establish a vertical emittance below 10 pmrad.

## INTRODUCTION

For emittance measurements on a synchrotron radiation (SR) source, an image formation method is most often used. Thus, the emittance determination relies on a beam size measurement, and knowledge of the machine functions. A successful measurement of the beam size needs a) a good optic scheme resulting in a near distortion-free image and b) a model for SR emission and propagation through the optics to find the relation between image and actual beam size. At SLS we have realized two optics schemes which observe (almost) the same point within a bending magnet. One such scheme is the well known pinhole camera using SR X-rays (ex. [1]). The other uses focused vertically polarized visible-to-UV SR, a technique developed at MAX-lab [2].

The model we use to describe the two optics schemes is based on a near-field calculation, using the retarded potentials, of the SR electromagnetic fields at the first optical element. Preserving all phase information, the fields are then propagated, through pinhole/lens and other apertures, within the frame of scalar diffraction theory. Finally the intensity distribution is calculated in the image plane. This distribution, resulting from a single relativistic electron, is termed the “filament-beam-spread-function” (FBSF). It is the equivalent to point-spread-functions in the case of virtual point sources. Convoluting the FBSF with a Gaussian distribution (or any assumed electron distribution) gives the measured image profile. The SRW-

code [3], used for our calculations, is based on this model. In the case of focused vertically polarised light the FBSF - in the vertical direction - is a two-peaked distribution with a zero minima in the centre (for 2-dim. visualisation please see [4]). For an increasing vertical beam size this minimum becomes shallower, allowing for a sensitive beam size determination. A vertically thin absorber blocks the intense mid-part of SR in our optical scheme. It is included in the modelling, but only marginally affects the FBSF. In the pinhole camera case, the result is a FBSF with a slightly smaller width than the one given from the approximate approach of ‘adding in square’ contributions from Fraunhofer diffraction and geometrical blurring due to the finite pinhole size.

## THE DIAGNOSTIC BEAMLIN

The source point of the beam line is the centre of the middle bending magnet in the SLS triple bend achromat lattice (see Table 1 for machine parameters). The X-ray branch uses only 0.8 mrad<sub>H</sub>, while the visible branch, immediately next to it, has a clearance of 7.0 mrad<sub>H</sub> x 8.8 mrad<sub>V</sub>. The water cooled pinhole array, fabricated from a 150 $\mu\text{m}$  thick Tungsten sheet with 15 $\mu\text{m}$  diameter holes, is located 4.022 m from the source point (sp). The light escaping these holes carries negligible power and is released through a 250 $\mu\text{m}$  thick Aluminium window.

In the visible branch the light is twice directed through 90° angles to achieve parallelism with the X-rays at a separation of 0.35m. The first mirror is made of SiC, a material which has a very advantageous ratio of thermal conductivity and expansion. This helps in low current measurements for moderate heat loads (a few tens of Watts). However it is stressed that for higher currents a “thin absorber” has been inserted before the mirror, while obstructing only the mid  $\pm 0.45$  mrad<sub>V</sub> of the SR. This takes away almost all the 400 Watt heat load on the mirror at full current, avoiding mirror deformation. The second mirror is a movable aluminized fused silica (FS) mirror. A FS spherical lens (5.076m from sp) is positioned between the two mirrors. These three optical components are chosen with  $\lambda/20$  surface accuracy. One vertically, and two horizontally movable blocking blades are situated near the lens to vary the acceptance angles. The visible-to-UV light is brought out of vacuum only at the end of the beam line (~9m from sp), through a FS window.

Monochromating Molybdenum filters and phosphor (P43) for the X-ray branch, grey filters, bandpass (BP) filters, a polarizer for the visible branch and the two Firewire, “Pointgrey Flea”, CCD cameras (pixel size 4.65  $\mu\text{m}$ ) are placed on an optical table at the end of the beam line. The visible branch camera can be remotely moved longitudinally when different BP filters are used, since the

lens' focal length is wavelength dependant; the X-ray branch camera has a zoom and focus adjustable lens system. The magnification of the two optical schemes are 0.840/0.854 (at 364/403 nm) and 1.276 (to phosphor).

Table 1: Some SLS parameters

Energy	2.4 GeV
Dipole field	1.4 T
Nat. Energy Spread	0.086%
$\beta_x ; \beta_y ; \eta_x$ (at obs.point)	0.45 m; 14.3 m; 29 mm
Nom. Hor. Emittance FEMTO-wiggler [5] open/closed	5.5/7.3 nmrad
$\sigma_{x\text{theory}}$ (at obs.point)	56/62 $\mu\text{m}$

## MEASUREMENTS

Fig. 1 shows the beam size application displaying the visible branch. Data is updated at a rate of approx. 1 Hz. The scales are in pixel units, while the  $X_{\text{sig}}$  and  $Y_{\text{sig}}$  values presented are the derived electron beam rms values,  $\sigma_{\text{ex}}$  and  $\sigma_{\text{ez}}$ .  $\sigma_{\text{ez}}$  is derived from the summation of the pixel intensities within the red lines. The valley-to-peak intensity ratio (blue lines) is then converted by a pre-SRW-calculated table to  $\sigma_{\text{ez}} \cdot \sigma_{\text{ex}}$  is arrived at after integrating over the whole image spot, determining the FWHM value, and again converting by help of pre-SRW-calculations to  $\sigma_{\text{ex}}$ . A similar window can be opened for the X-ray branch.

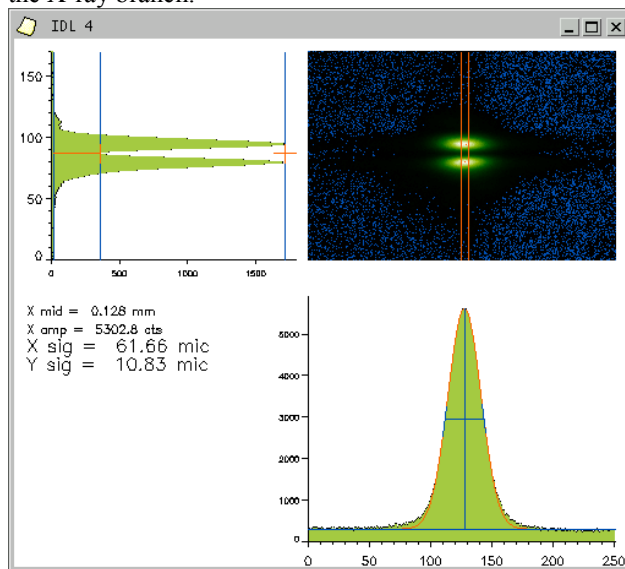


Figure 1: Image from the visible-to-UV branch. Vertically polarized at 403 nm. Machine conditions (M.c's): 350 mA, user top-up mode, FEMTO (F)-wiggler closed.

### Vis-to-UV Branch

Even though it is more challenging to determine the vertical beam size, it is also of great interest to verify that the model predictions also agree with measurements in the horizontal case, where usually the beam size is much larger. To explore this we measured horizontal image profiles - still with the setup for vertically polarized light - for different horizontal apertures set by the blocking blades at the lens position.

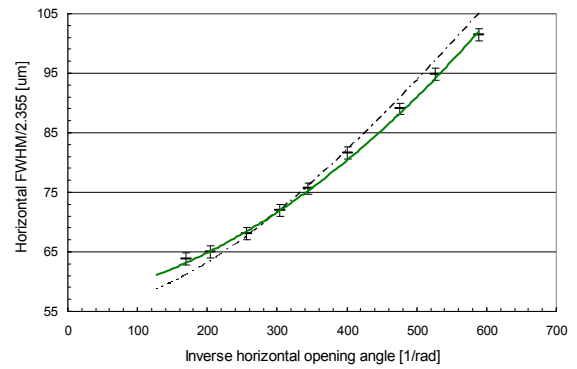


Figure 2: Measured (marks) and predicted (solid line) FWHM/2.355-values at 403 nm. M.c's: 350 mA, user top-up mode, F-wiggler open.

Fig. 2 shows the results, where we have plotted measured and predicted FWHM/2.355 of the images, against the inverse accepted horizontal SR opening angle. The solid line is the prediction from SRW, which is a convolution of a  $\sigma_{\text{ex}} = 55.6 \mu\text{m}$  Gaussian electron beam shape and the calculated FBSF for the different opening angles. We have also indicated (dashed line) the result given from simply adding in square the electron beam width and a  $(\sin/x)^2$  width resulting from the simplified assumption of treating the filament beam as a far away point source (Fraunhofer diffraction case). Discrepancies for small hor. acceptance angles originate only from the simplified 'adding in square' method instead of performing a pure convolution. Hence, a Fraunhofer approach is valid in this acceptance region. For large acceptance angles the deviation is additionally due to the more complicated phase relations of the SR electric field emission over the arc, compared to a virtual point source, making the Fraunhofer approach invalid.

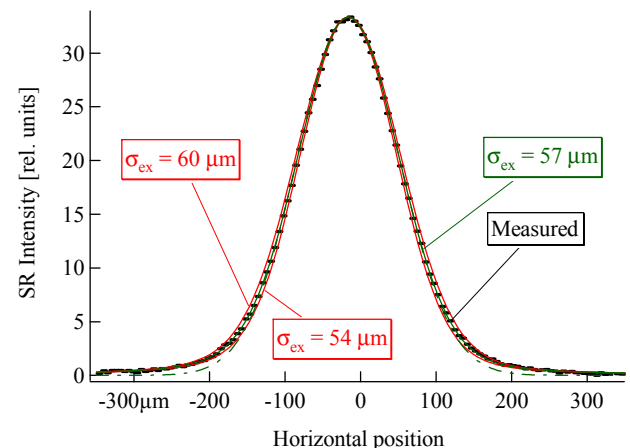


Figure 3: Measured (marks) and predicted (solid lines) horizontal profile at 364 nm, 3.9 mrad<sub>H</sub>. M.c's: 350 mA in user top-up mode, F-wiggler open.

Fig. 3 shows an example of an entire horizontal image profile. The lines are profile predictions calculated from the SRW model by convoluting the FBSF with a Gaussian electron beam and afterwards integrating over the entire image, as done with the on-line monitor. Of particular

note is the good agreement in the tails, which clearly deviates from a Gaussian shape (dashed line).

As an example of the vertical beam size measurement performed with vertically polarized light we present a profile (Fig. 4) obtained at 350 mA circulating current. SLS was for several weeks operated in standard user mode with these beam properties. This mode, with carefully tuned sqew quadrupole settings, gave the smallest vertical rms beam size,  $\sigma_{ez} = (7.5 \pm 0.5) \mu\text{m}$  at the monitor. This corresponds to a vertical emittance of,  $\epsilon_z = (3.9 \pm 0.7) \text{ pmrad}$ , the smallest so far reached at SLS. Again, the SRW model predicts very well the profile - peak widths correspond to valley depth. However, the example shows that we start to reach the limit resolution of the method. The slightly raised intensity levels in the tails most probably originate from one or several non-ideal optics element. Such a contribution in the intensity valley can therefore not be excluded. The estimated vert. beam size is hence an upper estimation of the real size.

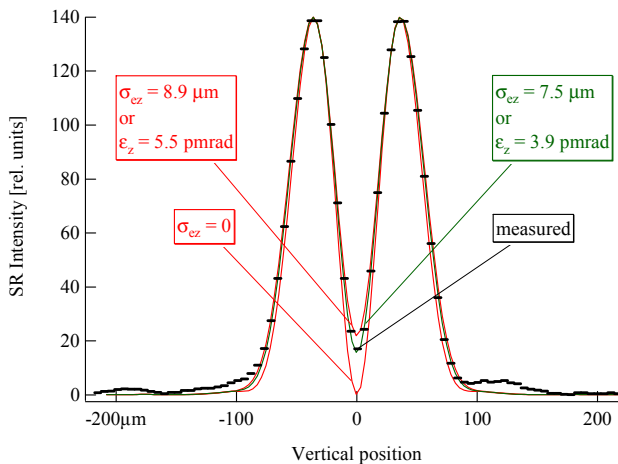


Figure 4: Measured (marks) and predicted (solid lines) vertical profile at 364 nm, 3.9 mrad<sub>H</sub>. M.c's: 350 mA in user top-up mode, F-wiggler open, tuned sqew quads.

To circumvent this problem one could either block a major part of the central SR, or detect at shorter wavelengths. Both methods bring the peaks of the FBSF closer together, making the valley to peak intensity ratio more prone to smaller beam sizes. We prefer the latter method, since it preserves the possibility to cross-check the optics quality from the tails behaviour. In the former case, one is essentially moving towards a pure interferometric [6] method, where tails and possible beam rotations are being obscured by a growing fringe pattern.

In order to cross-check the model predictions, in a fashion similar to that for the horizontal case, the vertically blocking blade is used, making the SR contribution to the image asymmetric. No contradictions have so far been made evident.

### X-Ray Branch

The X-ray branch has also been modelled by the SRW code for monochromatic 16 keV SR, giving a FBSF of 9  $\mu\text{m}$  FWHM/2.355, in both directions (converted to 1:1 imaging). The vertical spot size FWHM/2.355 obtained

for the above mentioned SLS conditions was 13.7  $\mu\text{m}$ . De-convolution gives  $\sigma_{ez} = 10 \mu\text{m}$ . This is however not necessarily in contradiction to the visible branch result, since chromatic effects and phosphor related effects are excluded. Phosphor thickness and phosphor grain size contributes to the final image to as yet unquantified extent. In the near future we will install pinholes of different sizes in order to systematically compare measured profiles with the model predictions, as done in the visible branch. An advantage of the X-ray branch is that small beam rotations can be quantified. A drawback, compared to the visible branch, is the over-all light yield, which is between  $10^3$  and  $10^4$  times lower, preventing us from making fast and/or low current measurements.

### Combined Measurements

Even though the X-ray branch does not yet reach the same resolution as the visible branch, it serves as a perfect complement in order to verify tiny ( $< 0.5 \mu\text{m}$ ) beam size changes during machine operation. If seen on both monitors, one can most often exclude measurement artefacts, as the cause of change. In this way it has been possible to search, and find, the cause of several tiny beam size alterations.

## CONCLUSION

A method utilizing vertically polarised visible-to-UV SR has been implemented to determine the vertical beam size at SLS. For the so far best tuned sqew quadrupole setting found, at 350 mA top-up mode, the upper limit of the rms beam size at the monitor was determined to be  $\sigma_{ez} = (7.5 \pm 0.5) \mu\text{m}$ . This corresponds to a vertical emittance of,  $\epsilon_z = (3.9 \pm 0.7) \text{ pmrad}$  including possible vertical beta function errors. An X-ray pinhole camera setup measures at the same source point  $\sigma_{ez} = 10 \mu\text{m}$ . In this case, possible chromatic and phosphor related effects have to be further explored to determine their error contribution. The two monitors have served to provide important feedback to machine operators regarding the electron beam size, and have helped to establish a vertical emittance of less than 10 pmrad, for standard user operation at the SLS.

## REFERENCES

- [1] P. Elleaume et.al., J. Synchrotron Rad.(1995)2, p.209
- [2] Å. Andersson, Ph.D. thesis work (1997), ISBN 91-628-2686-7, and Å. Andersson, M. Eriksson, O. Chubar, EPAC'96, p. 1689.
- [3] O. Chubar, P. Elleaume, EPAC'98, p. 1177.
- [4] O. Chubar, P. Elleaume, A. Snigerev, Nucl. Instr. And Meth. A 435 (1999), p. 495.
- [5] A. Streun et. al, "Sub-picosecond X-ray Source FEMTO at SLS", EPAC'06, p. 3427.
- [6] T. Mitsuhashi, PAC'97, p. 766.